This is a preprint, the final version is subject to change, of the American Mineralogist (MSA)
Cite as Authors (Year) Title. American Mineralogist, in press.
(DOI will not work until issue is live.) DOI: http://dx.doi.org/10.2138/am-2017-6035

Revision 1

Spin state and electronic environment of iron in basaltic glass in the lower mantle

Fumiya Maeda[1], Seiji Kamada[1,2], Eiji Ohtani[1], Naohisa Hirao[3], Takaya Mitsui[4], Ryo Masuda[5], Masaaki Miyahara[6], and Catherine McCammon[7]

[1]Department of Earth Science, Graduate School of Science, Tohoku University, Sendai, 980-8578, Japan.

[2]Frontier Research Institute for Interdisciplinary Sciences, Tohoku University, Sendai, 980-8578, Japan.

[3]Japan Synchrotron Radiation Research Institute, Hyogo, 679-5198, Japan.

[4]Synchrotron Radiation Research Center, Kansai Photon Science Institute, Quantum Beam Science Research Directorate, National Institutes for Quantum and Radiological Science and Technology, Hyogo, 679-5148, Japan.

[5]Research Reactor Institute, Kyoto University, Osaka, 590-0494, Japan.

[6]Department of Earth and Planetary Systems Science, Graduate School of Science,

Hiroshima University, Hiroshima, 739-8526, Japan.

[7]Bayerisches Geoinstitut, University of Bayreuth, Bayreuth, 95440 Germany.

Abstract

The spin states of iron in deep magmas are one of the most important properties that affect the partitioning of iron between magmas and minerals, and thus the gravitational stability of magmas in the Earth. We investigated the spin state and electronic environments of iron in a basaltic glass at room temperature and pressures from 1 bar to 130 GPa using a diamond anvil cell combined with energy domain synchrotron ^{57}Fe Mössbauer source spectroscopy. The basaltic glass represents an analog of a multi-component magma typical for the Earth. The Mössbauer spectra could be fitted by a two pseudo-Voigt doublet model including a high quadrupole splitting (QS) doublet and a low QS doublet, which were assigned to high-spin Fe^{2+} and high-spin Fe^{3+}, respectively. The high-spin states of Fe^{2+} and Fe^{3+} remained up to 130 GPa corresponding to the pressure in the lowermost mantle. The center shift values of high-spin Fe^{2+} and Fe^{3+} did not show large changes with pressure, ruling out sharp electronic changes in the basaltic glass. Therefore, a sharp and complete

spin crossover of Fe^{2+} from the high spin to the low spin state does not appear to occur in the basaltic glass although the possibility of a partial spin transition cannot be fully excluded. The QS values of Fe^{2+} increased slightly at 0–20 GPa and above 100 GPa, and the higher value was preserved after decompression to ambient conditions. This behavior may be related to distortion of Fe^{2+} polyhedra due to short-range ordering on compression. Such a distortion of Fe^{2+} polyhedra could gradually stabilize Fe^{2+} in the basaltic glass with pressure compared to bridgmanite according to the Jahn–Teller effect, and thus could gradually enhance the partitioning of iron into deep magmas in the lower mantle.

Keywords: Silicate glass, deep magma, spin transition, lower mantle, synchrotron Mössbauer spectroscopy, diamond anvil cell

Introduction

The existence of magmas in the deep Earth is important for understanding deep Earth processes and evolution of the Earth. New geophysical observations and advances in high-pressure and high-temperature experiments have provided new insight on deep magmatism in the Earth's mantle (e.g., Andrault et al. 2014; Kawakatsu et al. 2011; Lay et

al. 2004; Ohtani and Maeda 2001; Pradhan et al. 2015; Sakamaki et al. 2013; Schmandt et al. 2014; Schmerr 2012; Song et al. 2004; Williams and Garnero 1996). Since partial melting can explain seismic velocity anomalies of ultra-low velocity zones (ULVZ) in the lowermost mantle, dense deep magmas have been considered to exist above the core-mantle boundary (CMB) (e.g., Berryman 2000; Lay et al. 2004; Komabayashi et al. 2009; Ohtani and Maeda 2001; Williams and Garnero 1996). Such deep magmas may cause super-plumes relating to hot spots (e.g., Lay et al. 2004; Murakami et al. 2014). On the other hand, the observed anomalies in the lowermost mantle have also been explained by the existence of metallic iron from the outer core (Otsuka and Karato 2012).

The controversies regarding the ULVZ arise partly from a lack of knowledge about the stability of deep magmas. In order to discuss the possible existence of deep magmas, we need to understand the physical and chemical properties of magmas under extreme high-pressure conditions. For instance, the gravitational stability of deep magmas can depend on the density contrast between solid and melt (e.g., Ohtani and Maeda 2001; Agee and Walker 1993) or the permeability of the melt through mantle mineral assemblages (i.e., dihedral angles between melt and minerals). However, magmas are technically difficult to

study in high-pressure and high-temperature experiments. As an alternative, silicate glasses have been used as analogs of deep magmas because they are considered to preserve the structures of quenched silicate melts (e.g., Lee, 2011; Lee et al. 2012; Williams and Jeanloz 1988).

The spin state of iron is one of the most important factors affecting the gravitational stability of deep magmas because iron is an abundant and relatively dense element among the major elements of the Earth. The partitioning of iron into silicate melt was reported to be enhanced at pressures greater than ~76 GPa, which could cause the formation of iron-rich dense melt above the CMB (Nomura et al. 2011). Nomura et al. (2011) suggested that iron partitioning between solid and liquid can be changed due to spin crossover of iron from the high-spin (HS) to the low-spin (LS) state occurring around 70 GPa. On the other hand, several recent studies have suggested that the HS-LS transition might not occur in a narrow pressure range in silicate glass at pressures corresponding to the Earth's lower mantle (e.g., Gu et al. 2012; Mao et al. 2014; Murakami et al. 2014; Prescher et al. 2014). Moreover, no spin transition has been suggested in silicate glasses (Mao et al. 2014; Prescher et al. 2014). However, an intermediate-spin (IS) state of Fe^{2+},

defined as the electron configuration with two unpaired *d* electrons, was recently observed in $(Mg,Fe)SiO_3$ glass above 20 GPa using Mössbauer spectroscopy, and a gradual HS-IS transition has been suggested under the pressure in the lower mantle (Murakami et al. 2014).

Previous studies have discussed the spin state of iron in simple-component glasses, for example, $(Mg,Fe)(Si,Al)O_3$ glass (Gu et al. 2012; Mao et al. 2014; Murakami et al. 2014; Nomura et al. 2011; Prescher et al. 2014) or $(Na,Fe)Si_2O_6$ glass (Prescher et al. 2014). Since the deep interior of the Earth likely involves multi-component systems, such complex systems should be studied in order to obtain realistic results for deep magmas. In this study we focused on a basaltic glass with composition typical for the Earth and measured the spin states of iron in this glass at pressures up to about 130 GPa, corresponding to the pressure in the lowermost mantle. The spin states of iron were measured using energy domain synchrotron ^{57}Fe Mössbauer source spectroscopy, which provides direct information on the electronic environments of iron.

Experimental methods

97 The starting material was a synthesized ^{57}Fe-enriched basaltic glass (Table 1). The
98 basaltic glass was prepared by quenching a molten mixture of oxides and carbonates; SiO_2,
99 MgO, Al_2O_3, TiO_2, $^{57}Fe_2O_3$ (96.64 % ^{57}Fe, ISOFLEX) and $CaCO_3$, K_2CO_3, Na_2CO_3. The
100 mixture was ground with an alumina mortar and melted in a gas-mixing furnace in a
101 controlled H_2-CO_2 atmosphere at 1673 K for 5 min. The oxygen fugacity was adjusted to
102 the conditions of coexistence of metallic iron and ferrous iron with approximately $\log fO_2$ =
103 -10.5. The quenched glass was ground again to make a chemically homogeneous powder.
104 The composition of the glass was analyzed using a field emission-scanning electron
105 microscope (FE-SEM), JEOL JSM-7100F, operating at 15 kV and equipped with an energy
106 dispersive X-ray spectroscopic (EDS) detector, Oxford Inca.
107 High-pressure experiments were performed using a symmetric-type diamond anvil
108 cell (DAC). The culet size of the diamonds was 150 μm in diameter. Tungsten was used as
109 a gasket, and was pre-intended to a thickness of 50 μm with a 70-μm hole as a sample
110 chamber. The hole was drilled using a Nd: YAG laser. The silicate glass powder was
111 sandwiched between NaCl pellets which worked as a pressure medium and a pressure scale.
112 The pressure was determined based on the pressure dependence of the diamond T_{2g} mode in

the experiments (Akahama and Kawamura 2004).

Energy domain synchrotron ^{57}Fe Mössbauer source (SMS) spectroscopy was conducted at beamlines BL10XU and BL11XU of SPring-8 at room temperature and pressures ranging from 1 atm to 130 GPa. A SMS with a $^{57}FeBO_3$ (111) nuclear Bragg monochromator is useful to study a small specimen in a DAC (Mitsui et al. 2009; Potapkin et al. 2012). The Doppler velocity scales were calibrated using a 3-μm thick piece of α-^{57}Fe foil under ambient conditions. Spectra were collected for 3–11 hours depending on the signal quality. The obtained Mössbauer spectra were fitted with pseudo-Voigt lineshape doublets (e.g., Alberto et al. 1996; Lagarec and Rancourt 1997) using the MossA software package (Prescher et al. 2012). This fitting model empirically explains well the lineshape of the ferric doublet in basaltic glasses (Partzsch et al. 2004). Ferrous doublets are often fitted assuming distributions of hyperfine parameters. However, the present glass has a high ferric content ($Fe^{3+}/\Sigma Fe \sim 0.66$) and therefore the shape of the ferrous iron doublet is not well constrained by the data. Without constraints on the correlation between center shift (CS) and quadrupole splitting (QS) (Fig. 1), unrealistic values often result (e.g., negative correlation between CS and QS). We therefore assumed zero correlation (i.e., assuming no

129 distributions in CS) for the ferrous iron doublet and obtained plausible fitting results that
130 are consistent with previous studies (e.g., Alberto et al. 1996; Partzsch et al. 2004).

131 A thin foil was prepared from the sample recovered after quenching from 130 GPa
132 to ambient conditions using a focused ion beam (FIB) system, JEOL JEM-9320FIB, and
133 observed using a field emission-gun transmission electron microscope (FE-TEM), JEOL
134 JEM-2100F, operating at 200 kV at Tohoku University. The thin foil (~10 μm × 3 μm × 1
135 μm) was extracted from the center of the sample chamber first, and then thinned to ~100
136 nm in thickness. The Ga ion beam was accelerated to 30 kV. The detailed FIB procedures
137 are described by Miyahara et al. (2008).

138

139 **Results**

140 Figure 1 shows representative Mössbauer spectra at 1 atm and high pressures. The
141 obtained Mössbauer spectra were fitted using a two-doublet model, one with higher
142 quadrupole splitting (QS: 1.9–2.9 mm/s) and one with lower QS (1.2–1.8 mm/s). The high
143 and low QS doublets are assigned to HS Fe^{2+} and HS Fe^{3+}, respectively, from comparison
144 of QS and center shift (CS) values with those of HS Fe^{2+} and Fe^{3+} reported by Dyar et al.

(1985) and of HS and IS Fe^{2+} in Murakami et al. (2014) (Fig. 2).

The CS values of the two doublets show relatively small changes with pressure compared to the CS decrease caused by the HS-IS transition, and thus they are almost constant on compression and after decompression to ambient pressure (Figs. 2, 3a). This behavior suggests that there are no abrupt electronic transitions involving the two iron species in the glass up to 130 GPa. The QS values of the two doublets show some increase from 1 bar to 130 GPa (Fig. 3b). The QS of HS Fe^{2+} slightly increases at pressures up to ~20 GPa and above 100 GPa with somewhat steeper gradients. The QS increase of HS Fe^{3+} is smaller and thus QS is not as sensitive to pressure. The QS of Fe^{2+} is higher in the recovered sample than in the starting material (Figs. 3b, 4). QS of Fe^{2+} therefore changes irreversibly with pressure while CS of Fe^{2+} and CS and QS of Fe^{3+} are reversible (Fig. 3a, b). The area ratios of Fe^{2+} and Fe^{3+} ($Fe^{2+}/\Sigma Fe$ and $Fe^{3+}/\Sigma Fe$) do not change with pressure within fitting uncertainties (Fig. 3c). Nevertheless, the $Fe^{2+}/\Sigma Fe$ ratio of the recovered sample is slightly less than the starting value. Therefore we considered the possibility of the iron disproportionation reaction: $3Fe^{2+} \rightarrow 2Fe^{3+} + Fe^{0}$ (e.g., Frost et al. 2004; Miyajima et al. 1999) and investigated the recovered sample using TEM. We confirmed that no

161 crystalline products were present in the recovered glass based on the selected area electron
162 diffraction pattern and the bright field image (Fig. 5), and thus we do not consider that the
163 iron disproportionation reaction occurred to any observable extent.
164
165 **Discussion**
166 **Spin states of iron under high-pressure conditions in silicate glasses.**
167 The present Mössbauer spectra can be fitted to a two-doublet model over the entire
168 pressure range and the CS values of Fe^{2+} and Fe^{3+} do not show a large change with pressure.
169 Therefore, there is no clear evidence for a sharp spin crossover of ferrous iron (e.g., spin
170 collapse around 70 GPa: Nomura et al. 2011) at any pressure within the lower mantle. This
171 conclusion is consistent with recent studies of silicate glasses that also show no evidence
172 for spin crossover (Mao et al. 2014; Prescher et al. 2014). On the other hand, some recent
173 studies reported gradual spin transitions of HS Fe^{2+} in silicate glasses (Gu et al. 2012;
174 Murakami et al. 2014; Ramo and Stixrude 2014). They reported HS-LS and/or HS-IS
175 transitions of ferrous iron that occurred over a broad pressure range. From the present
176 results we cannot rule out such a partial and gradual spin transition. Moreover, the large

177 proportion of Fe^{3+} could make it difficult to detect a lower spin-number component in this
178 study, since IS Fe^{2+} might partially overlap with HS Fe^{3+} in the spectra during such a spin
179 transition. Although such subtle spin transitions from HS Fe^{2+} to LS or IS Fe^{2+} cannot be
180 completely excluded, our data support the conclusion that HS Fe^{2+} and HS Fe^{3+} are the
181 main iron species in the present basaltic glass up to 130 GPa.
182
183 **Relation between hyperfine parameters and structure on compression.**
184 Hyper-fine parameters and the structure of glasses are closely related with each
185 other. The CS is sensitive to the *s*-electron density at the iron nucleus, which directly relates
186 to the Fe-O distances of iron polyhedra. Changes of CS on compression can be caused by
187 two possible changes of Fe-O polyhedra: reduced Fe-O distances and increased
188 coordination numbers of the polyhedra. Since the reduction of the Fe-O distances can
189 increase *s*-electron density at the nucleus and hence decrease CS, CS becomes smaller on
190 simple compression of Fe-O polyhedra. On the other hand, CS enhancement can occur
191 when the coordination number of Fe increases and Fe-O bonds are elongated. Changes of
192 coordination number can occur over wide pressure ranges in the case of silicate glasses

193 (e.g., Bajgain et al. 2015; Sanloup et al. 2013). Therefore, the effect of pressure on CS is
194 determined by a competition between the effects of Fe-O shortening and gradual
195 coordination increase in silicate glasses.

196 The CS of Fe^{2+} and Fe^{3+} shows only minor changes with increasing pressure in the
197 present basaltic glass compared with the drop in CS at the HS-IS transition (Fig. 2:
198 Murakami et al. 2014). The CS of HS Fe^{2+} decreases slightly at 20–60 GPa and then
199 increases between 60 and 80 GPa. A decrease of ferrous CS has also been reported at
200 similar pressures in previous studies (Prescher et al. 2014; Rouquette et al. 2008). Prescher
201 et al. (2014) observed a decreasing tendency of Fe^{2+} CS below 50 GPa. They explained this
202 tendency by the stronger influence of compression compared to the coordination increase of
203 Fe^{2+} up to 50 GPa with a possible change in compression mechanism below 50 GPa. Such a
204 change in compression mechanism could be caused by the increase of Si coordination
205 number from 4 to 6 reported in silicate glasses, which can be nearly finished around 50 GPa
206 (e.g., Murakami and Bass 2010; 2011; Prescher et al. 2014; Sanloup et al. 2013; Sato and
207 Funamori 2008; 2010). The intense compression of silicate glasses was reported up to 20
208 GPa to be related to an Si-coordination increase (Wakabayashi et al. 2011; 2015). A recent

ab initio study showed a coordination number increase in Fe^{2+} up to 40 GPa, which contributes to the increase of Fe^{2+} CS. Therefore, the present CS decrease might be the result of the stronger compression effect related to Si-coordination increase rather than a coordination-increase effect in Fe^{2+} (Wakabayashi et al. 2011; 2015). The coordination number of Fe^{2+} was reported to increase slightly between 50 and 80 GPa (Bajgain et al. 2015). The subtle CS increase in this study might be related to a small coordination change. The Fe^{2+} CS becames almost constant with pressure and decreases above 120 GPa. The invariance of CS around 100 GPa might be related to a trade-off between compression and increase of coordination number. The Si coordination number has been suggested to increase above 100 GPa in silicate glasses, which may be related to a coordination change of Fe around 100 GPa (e.g., Murakami and Bass 2010; 2011; Ohira et al. 2016). The CS of Fe^{3+} shows almost no dependence on pressure apart from a slight decrease with increasing pressure. The CS of Fe^{3+} may therefore record only the compression effect of Fe^{3+} polyhedra.

The QS is sensitive to the electric field gradient at the iron nucleus, which is influenced by the asymmetry of the coordination polyhedron and/or the electronic

distribution. The QS of Fe^{2+} generally increases with distortion of the Fe-O coordination polyhedron but it decreases at the Fe^{2+} HS-IS transition to almost the same values as the QS of HS Fe^{3+} in the case of silicate glass (Murakami et al. 2014). The QS of HS Fe^{2+} in the present glass increases somewhat up to 20 GPa and between 100 and 130 GPa. This tendency may be caused by a distortion of Fe^{2+} polyhedra related to short-range ordering that occurs during compression (e.g., Kantor et al. 2009). An increase of coordination number of Si and Fe is expected at these pressures (e.g., Bajgain et al. 2015; Murakami and Bass 2010; 2011; Ohira et al. 2016; Sanloup et al. 2013; Sato and Funamori 2008; 2010). The Si coordination increase was suggested to originate from the change of Si-O-Si angles and distortion of the SiO_4 tetrahedra in silicate glasses (Stolper and Ahrens 1987). The coordination change might also be related to the distortion of Fe polyhedra. If distorted polyhedra existed during the continuous structural changes in the glass, Fe might prefer distorted sites because their energies are lower than non-distorted ones according to the Jahn–Teller effect. Such short-range ordering was observed to be preserved after quenching to ambient pressure for (Mg,Fe)O (Kantor et al. 2009). The larger QS of Fe^{2+} in the present recovered sample is comparable to the value at high pressure (Fig. 3). This observation

might also be evidence of short-range ordering in the basaltic glass.

Fe^{2+} QS decreases between 80 and 100 GPa, while Fe^{2+} CS slightly increases in the same pressure range (Fig. 3). This behavior differs from previous observations of the HS-IS spin transition in a silicate glass where both Fe^{2+} CS and QS decrease (Murakami et al. 2014); hence the spin transition can be excluded as the cause of the Fe^{2+} QS decrease. Experiments and calculations indicate that structural changes might be small in silicate glasses within this pressure range (e.g., Bajgain et al. 2015; Sanloup et al. 2013; Murakami and Bass 2011). Therefore, Fe^{2+} QS might show the opposite tendency to short-range ordering after forming higher coordination polyhedra and without structural changes between 80 and 100 GPa.

Relative area ratios of Fe^{2+} and Fe^{3+}.

The relative abundance of iron species in the basaltic glass as measured by their relative areas does not change with pressure within experimental uncertainty (Fig. 3c), although visually the relative area of the Fe^{2+} component appears smaller at the highest pressure and in the recovered sample (Fig. 1). Considering the large uncertainties in fitted

areas and that two previous studies reported an apparent decrease of $Fe^{2+}/\sum Fe$ with pressure in silicate glasses (Gu et al. 2012; Prescher et al. 2014), we examine more carefully the case for a decrease of $Fe^{2+}/\sum Fe$. We distinguish between effects that change the relative areas of Fe^{2+} and Fe^{3+} components while relative abundance remains constant, and effects that do change their relative abundance.

Previous studies suggested that the relative area of the Fe^{2+} doublet could decrease due to: (i) HS-LS spin transition of Fe^{2+} with overlap of HS Fe^{3+} and LS Fe^{2+}, and/or (ii) different changes in the recoil-free fractions of Fe^{2+} and Fe^{3+} with pressure (Gu et al. 2012; Prescher et al. 2014). An argument against both of these effects is the important observation that the relative area of Fe^{2+} remains smaller after quenching in both the present study and that of Prescher et al. (2014). This observation rules out both possibilities because spin transitions and effects leading to changes in recoil-free fraction are not preserved on decompression to ambient conditions. Previous studies further suggested that $Fe^{2+}/\sum Fe$ could decrease through iron disproportionation and/or pressure-induced oxidation of Fe^{2+} (Prescher et al. 2014). Since we confirmed (see above) the lack of evidence for iron disproportionation using TEM and iron oxidation is not expected to occur at room

temperature, these possibilities can also be ruled out.

We propose a further possibility to explain an apparent decrease in the relative area of the Fe^{2+} component without changing the abundance of Fe^{2+}, namely electron hopping between Fe^{2+} and Fe^{3+}. Such an electron exchange between Fe^{2+} and Fe^{3+} could result in a virtual valence state of Fe^{n+} ($2<n<3$), which has been observed as a Mössbauer doublet in iron-bearing minerals at ambient conditions with CS intermediate between Fe^{2+} and Fe^{3+} (Amthauer and Rossman 1984; Fei et al. 1994). This electron change could occur between edge- or face-shared Fe^{2+} and Fe^{3+} polyhedra (e.g., Amthauer and Rossman 1984; Fei et al. 1994) and could be enhanced at high pressure (Morris and Williams 1997). Tetrahedral sites of Si were considered to share edges or faces in the process of coordination increase from 4 to 6 at high pressure (Stolper and Ahrens 1987). Such edge- or face-sharing in Fe^{2+} and Fe^{3+} polyhedra can be expected in the case of Fe^{2+} since its coordination number may also change from 4 to 6 (Bajgain et al. 2015). Coordination increase could hence promote electron hopping between Fe^{2+} and Fe^{3+}. In addition, silicate glasses have been reported to partially retain their densified structures after decompression (e.g., Ohtani et al. 1985; Xue et al. 1989; Wakabayashi et al. 2015). Therefore, Fe^{n+}

resulting from electron hopping enhanced by pressure could be preserved after decompression to ambient conditions in the basaltic glass. In this case the subspectra of Fe^{n+} and Fe^{3+} could overlap due to the broad linewidths of the Mössbauer spectra of silicate glass. In any event, such a minor change in relative areas does not influence the conclusion of our study.

Implications

The basaltic composition is typical for the Earth; thus basaltic glass has been used as an analog for the magmas in the deep Earth (e.g., Murakami et al. 2014; Ohtani and Maeda 2001). Deep magmas expected in the lowermost mantle may be generated by partial melting of the basaltic portion of subducted slabs in the lowermost mantle and are suggested to be richer in SiO_2 compared to the composition of mid-ocean ridge basalts (MORB) (Andrault et al. 2014). The basaltic glass used in the present study is more SiO_2-rich than MORB. Therefore it may be relevant for the magmas in the lowermost mantle that can cause seismic anomalies (e.g., Lay et al. 2004; Williams and Garnero 1996).

One of the most significant observations in the present study is the absence of a sharp spin crossover in Fe^{2+}, contrary to one suggested by Nomura et al. (2011) to occur around 59–77 GPa. We therefore do not predict iron enrichment in magmas through a sharp change in the magma-crystal partition coefficient, D_{Fe}(solid/liquid), caused by spin crossover of Fe^{2+} in magmas. On the other hand, Andrault et al. (2012) reports a gradual decrease of D_{Fe}(solid/liquid) on compression without any steep change up to pressures corresponding to the lowermost mantle conditions. This gradual change may be explained based on the present results in terms of a distortion of Fe^{2+} polyhedra, because the cation could be more stable in the distorted site according to the Jahn–Teller effect. As mentioned above, the slight increase of Fe^{2+} QS combined with the irreversible change of QS after decompression suggests increased short-range order in Fe^{2+} polyhedra. Such a distortion of Fe-O polyhedra can enhance the stability of octahedrally coordinated ferrous ion in the basaltic glass because of the Jahn–Teller splitting of the 3d orbitals (Burns 1993). In the case of $(Mg,Fe)(Si,Al)O_3$ bridgmanite, the main component of the lower mantle, the QS of each Fe species has been reported to decrease or remain almost constant on compression to lower-mantle pressures (e.g., Kupenko et al. 2015; Lin et al. 2012; McCammon et al. 2010).

This behavior may be an indication that Fe-O polyhedra in bridgmanite undergo less distortion than the present glass, and thus, Fe^{2+} in bridgmanite may have a higher energy than in the silicate glass in terms of the Jahn–Teller effect. Therefore, Fe may favor the silicate melt relative to minerals under lower mantle conditions, based on the consideration of the present glass as a structural analog to the multicomponent melt of Andrault et al. (2012). In addition, the slight and gradual change of QS with pressure is a common tendency of ferrous QS in the present study and the D_{Fe}(solid/liquid) decrease reported by Andrault et al. (2012) (Fig. 6). Moreover, the Fe^{2+} QS increase around 80 GPa and decrease above 100 GPa corresponds almost exactly to the decrease and increase of D_{Fe}(solid/liquid) in Andrault et al. (2012) (Fig. 6). These observations may also support a relation between the distortion of Fe-O polyhedra and the partitioning of iron.

We note that D_{Fe}(solid/liquid) can be affected by spin crossovers in mantle minerals (e.g., Fujino et al. 2014). A gradual HS-IS(LS) spin transition was reported for bridgmanite in previous Mössbauer studies (e.g., Kupenko et al. 2015; McCammon et al. 2008; 2010). On the other hand, we cannot rule out the possibility of a partial HS-IS transition in the basaltic glass. Therefore, the effect of the spin transition on

337 D_{Fe}(solid/liquid) may be moderated if the spin transitions occurred in both bridgmanite and
338 a silicate melt. Although the present results suggest that Jahn–Teller effects in basaltic
339 melts may play a greater role in iron partitioning in the lower mantle than the spin transition
340 in mantle minerals, more detailed work is required to understand the geophysical and
341 geochemical properties of deep magmas.
342

343 **Acknowledgments**

344 Nanami Suzuki, Maki Hamada, Tatsuya Sakamaki, Akio Suzuki (Tohoku
345 University) and Yasuo Ohishi (JASRI) contributed valuable discussion and technical
346 support during the experiments. Bjorn Mysen (Carnegie Institution of Washington) and
347 Clemens Prescher (University Cologne) provided valuable discussions and suggestions on
348 the manuscript. This work was supported by the Grant-in-Aid for Scientific Research to
349 E.O. (numbers 22000002 and 15H05748) from the Ministry of Education, Culture, Sports,
350 Science, and Technology of the Japanese Government, and by the International Research
351 and Training Group "Deep Earth Volatile Cycles" funded by the German Science
352 Foundation (grant number GRK 2156/1). The synchrotron radiation experiments were

353 performed at SPring-8 with the approval of the Japanese Radiation Research Institute
354 (Proposals 2014A0104, 2014A3516, 2014B0104, 2014B3519, 2015A0104, and
355 2015B0104). F.M. was supported by the International Joint Graduate Program in Earth and
356 Environmental Science (GP-EES), Tohoku University. This work and F.M. were supported
357 by the JSPS Japanese-German Graduate Externship.

358

359 **References cited**

360 Agee, C.B., and Walker, D. (1993) Olivine flotation in mantle melt. Earth and Planetary
361 Science Letters, 90, 144–156.
362 Alberto, H.V., Pinto da Cunha, J.L., Mysen, B.O., Gil, J.M., and Ayres de Campos, N.
363 (1996) Analysis of Mössbauer spectra of silicate glasses using a two-dimensional
364 Gaussian distribution of hyperfine parameters. Journal of Non-Crystalline Solids, 194,
365 48–57.
366 Akahama, Y., and Kawamura, H. (2004) High-pressure Raman spectroscopy of diamond
367 anvils to 250 GPa: Method for pressure determination in the multimegabar pressure
368 range. Journal of Applied Physics, 96, 3748–3751.

Amthauer, G., and Rossman, G.R. (1984) Mixed valence of iron in minerals with cation clusters. Physics and Chemistry of Minerals, 11, 37–51.

Andrault, D., Petitgirard, S., Nigro, G.L., Devidal, J.-L., Veronesi, G., Garbarino, G., and Mezouar, M. (2012) Solid–liquid iron partitioning in Earth's deep mantle. Nature, 487, 354–357.

Andrault, D., Pesce, G., Bouhifd, M.A., Bolfan-Casanova, N., Hénot, J.-M., and Mezouar, M. (2014) Melting of subducted basalt at the core-mantle boundary. Science, 344, 892–895.

Bajgain, S., Ghosh, D.B., and Karki, B.B. (2015) Structure and density of basaltic melts at mantle conditions from first-principles simulations. Nature Communications, 6:8578, DOI: 10.1038/ncomms9578.

Berryman, J.G. (2000) Seismic velocity decrement ratios for regions of partial melts in the lower mantle. Geophysical Research Letters, 27, 421–424.

Burns, R.G. (1993) Mineralogical Applications of Crystal Field Theory, 32–39 pp. Cambridge University Press, U.K.

Dyar, M.D. (1985) A review of Mössbauer data on inorganic glasses: the effects of

385 composition on iron valency and coordination. American Mineralogist, 70, 304–316.
386 Fei, Y., Virgo, D., Mysen, B.O., Wang, Y., and Mao, H.K. (1994) Temperature-dependent
387 electron delocalization in (Mg,Fe)SiO_3 perovskite. American Mineralogist, 79, 826–
388 837.
389 Frost, D.J., Liebske, C., Langenhorst, F., McCammon, C.A., Trønnes, R.G., and Rubie, D.
390 (2004) Experimental evidence for the existence of iron-rich metal in the Earth's lower
391 mantle. Nature, 428, 409–412.
392 Fujino, K., Nishio-Hamane, D., Nagai, T., Seto, Y., Kuwayama, Y., Whitaker, M., Ohfuji,
393 H., Shinmei, T., and Irifune, T. (2014) Spin transition, substitution, and partitioning of
394 iron in lower mantle minerals. Physics of the Earth and Planetary Interiors, 228, 186–
395 191.
396 Gu, C., Catalli, K., Grocholski, B., Gao, L., Alp, E., Chow, P., Xiao, Y., Cynn, H., Evans,
397 W.J., and Shim, S.-H. (2012) Electronic structure of iron in magnesium silicate glasses
398 at high pressure. Geophysical Research Letters, 39, L24304.
399 Kawakatsu, H., Kumar, P., Takei, Y., Shinohara, M., Kanazawa, T., Araki, E., and
400 Suyehiro, K. (2009) Seismic evidence for sharp lithosphere-asthenosphere boundaries

401 of oceanic plates. Science, 324, 499–502.

402 Komabayashi, T., Maruyama, S., and Rino, S. (2009) A speculation on the structure of the
403 D" layer: The growth of anti-crust at the core-mantle boundary through the subduction
404 history of the Earth. Gondwana Research, 15, 342–353.

405 Kupenko, I., McCammon, C., Sinmyo, R., Cerantola, V., Potapkin, V., Chumakov, A.I.,
406 Kantor, A., Rüffer, R., and Dubrovinsky, L. (2015) Oxidation state of the lower
407 mantle: *In situ* observations of the iron electronic configuration in bridgmanite at
408 extreme conditions. Earth and Planetary Science Letters, 423, 78–86.

409 Lagarec, K., and Rancourt, D.G. (1997) Extended Voigt-based analytic lineshape method
410 for determining N-dimensional correlated hyperfine parameter distributions in
411 Mössbauer spectroscopy. Nuclear Instruments and Methods in Physics Research B,
412 129, 266–280.

413 Lay, T., Garnero, E.J., and Williams, Q. (2004) Partial melting in a thermo-chemical
414 boundary layer at the base of the mantle. Physics of the Earth and Planetary Interiors,
415 146, 441–467.

416 Lee, S.K. (2011) Simplicity in melt densification in multicomponent magmatic reservoirs

417 in Earth's interior revealed by multinuclear magnetic resonance. Proceedings of
418 National Academy of Science, 108, 6847–6852.
419 Lee, S.K., Yi, Y.S., Cody, G.D., Mibe, K., Fei, Y., and Mysen, B.O. (2012) Effect of
420 network polymerization on the pressure-induced structural changes in Sodium
421 aluminosilicate glasses and melts: ^{27}Al and ^{17}O solid-state NMR study. The Journal of
422 Physical Chemistry C, 116, 2183–2191.
423 Lin, J.F., Alp, E.E., Mao, Z., Inoue, T., McCammon, C., Xiao, Y., Chow, P., and Zhao, J.
424 (2012) Electronic spin state of ferric and ferrous iron in the lower-mantle silicate
425 perovskite. American Mineralogist, 97, 592–597.
426 Mao, Z., Lin, J.F., Yang, J., Wu, J., Watson, H.C., Xiao, Y., Chow, P., and Zhao, J. (2014)
427 Spin and valence state of iron in Al-bearing silicate glass at high pressures studied by
428 synchrotron Mössbauer and X-ray emission spectroscopy. American Mineralogist, 99,
429 415–423.
430 McCammon, C., Dubrovinsky, L., Narygina, O., Kantor, I., Wu, X., Glazyrin, K., Sergueev,
431 I., and Chumakov, A.I. (2010) Low-spin Fe^{2+} in silicate perovskite and a possible layer
432 at the base of the lower mantle. Physics of the Earth and Planetary Interiors, 180, 215–

221.

Mitsui, T., Hirao, N., Ohishi, Y., Masuda, R., Nakamura, Y., Enoki, H., Sakaki, K., and Seto, M. (2009) Development of an energy-domain ^{57}Fe-Mössbauer spectrometer using synchrotron radiation and its application to ultrahigh-pressure studies with a diamond anvil cell. Journal of Synchrotron Radiation, 16, 723–729.

Miyajima, N., Fujino, K., Funamori, N., Kondo, T., and Yagi, T. (1999) Garnet-perovskite transformation under conditions of the Earth's lower mantle: an analytical transmission electron microscopy study. Physics of the Earth and Planetary Interiors, 116, 117–131.

Miyahara, M., Sakai, T., Ohtani, E., Kobayashi, Y., Kamada, S., Kondo, T., Nagase, T., Yoo, J.H., Nishijima, M., and Vashaei, Z. (2008) Application of FIB system to ultra-high-pressure Earth science. Journal of Mineralogical and Petrological Science, 103, 88–93.

Morris, E.R., and Williams, Q. (1997) Electrical resistivity of Fe_3O_4 to 48 GPa: Compression-induced changes in electron hopping at mantle pressures. Journal of Geophysical Research, 102, 18,139–18,148.

Murakami, M., and Bass, J.D. (2010) Spectroscopic evidence for ultrahigh-pressure

449 polymorphism in SiO_2 glass. Physical Review Letters, 104, 025504.

450 Murakami, M., and Bass, J.D. (2011) Evidence of denser $MgSiO_3$ glass above 133
451 gigapascal (GPa) and implications for remnants of ultradense silicate melt from a deep
452 magma ocean. Proceedings of the National Academy of Sciences of the United States
453 of America, 108, 17286–17289.

454 Murakami, M., Goncharov, A.F., Hirao, N., Masuda, R., Mitsui, T., Thomas, S.M., and
455 Bina, C.R. (2014) High-pressure radiative conductivity of dense silicate glasses with
456 potential implications for dark magmas. Nature Communications, 5:5428 doi:
457 10.1038/ncomms6428.

458 Nomura, R., Ozawa, H., Tateno, S., Hirose, K., Hernlund, J., Muto, S., Ishii, H., and
459 Hiraoka, N. (2011) Spin crossover and iron-rich silicate melt in the Earth's deep
460 mantle. Nature, 473, 199–202.

461 Ohira, I., Murakami, M., Kohara, S., Ohara, K., and Ohtani, E. (2016) Ultrahigh-pressure
462 acoustic wave velocities of SiO_2-Al_2O_3 glasses up to 200 GPa. Progress in Earth and
463 Planetary Science, 3:18.

464 Ohtani, E., Taulelle, F., and Angell, A. (1985) Al^{3+} coordination changes in liquid
465 aluminosilicates under pressure. Nature, 314, 78–81.
466 Ohtani, E., and Maeda, M. (2001) Density of basaltic melt at high pressure and stability of
467 the melt at the base of the lower mantle. Earth and Planetary Science Letters, 193, 69–
468 75.
469 Otsuka, K., and Karato, S. (2012) Deep penetration of molten iron into the mantle caused
470 by a morphological instability. Nature, 492, 243–246.
471 Partzsch, G.M., Lattard, D., and McCammon, C. (2004) Mössbauer spectroscopic
472 determination of Fe^{3+}/ Fe^{2+} in synthetic basaltic glass: a test of empirical fO_2 equations
473 under superliquidus and subliquidus conditions. Contributions to Mineralogy and
474 Petrology, 147, 565–580.
475 Potapkin, V., Chumakov, A.I., Smirnov, G.V., Celse, J.-P., Ruffer, R., McCammon, C., and
476 Dubrovinsky, L. (2012) The ^{57}Fe synchrotron Mössbauer source at the ESRF. Journal
477 of Synchrotron Radiation, 19, 559-569.

Pradhan, G.K., Fiquet, G., Siebert, J., Auzende, A.-L., Morard, G., Antonangeli, D., and Garbarino, G. (2015) Melting of MORB at core–mantle boundary. Earth and Planetary Science Letters, 431, 247–255.

Prescher, C., Weigel, C., McCammon, C., Narygina, O., Potapkin, V., Kupenko, I., Sinmyo, R., Chumakov, A.I., and Dubrovinsky, L. (2014) Iron spin state in silicate glass at high pressure: Implications for melts in the Earth's lower mantle. Earth and Planetary Science Letters, 385, 130–136.

Prescher, C., McCammon, C., and Dubrovinsky, L. (2012) *MossA*: a program for analyzing energy-domain Mössbauer spectra from conventional and synchrotron sources. Journal of Applied Crystallography. 45, 329–331.

Ramo, D.M., and Stixrude, L. (2014) Spin crossover in Fe_2SiO_4 liquid at high pressure. Geophysical Research Letters, 41, 4512–4518.

Rouquette, J., Kantor, I., McCammon, C.A., Dmitriev, V., and Dubrovinsky, L.S. High-pressure studies of $(Mg_{0.9}Fe_{0.1})_2SiO_4$ olivine using Raman spectroscopy, X-ray diffraction, and Mössbauer spectroscopy. Inorganic Chemistry, 47, 2668–2673.

493 Sakamaki, T., Suzuki, A., Ohtani, E., Terasaki, H., Urakawa, S., Katayama, Y., Funakoshi,
494 K., Wang, Y., Hernlund, J.W., and Ballmer, M.D. (2013) Ponded melt at the boundary
495 between the lithosphere and asthenosphere. Nature Geoscience, 6, 1041–1044.
496 Sanloup, C., Drewitt, J.W.E., Konôpková, Z., Dalladay-Simpson, P., Morton, D.M., Rai, N.,
497 van Westrenen, W., and Morgenroth, W. (2013) Structural change in molten basalt at
498 deep mantle conditions. Nature, 503, 104–107.
499 Sato, T., and Funamori, N. (2008) Sixfold-coordinated amorphous polymorph of SiO_2
500 under high pressure. Physical Review Letters, 101, 255502.
501 Sato, T., and Funamori, N. (2010) High-pressure structural transformation of SiO_2 glass up
502 to 100 GPa. Physical Review B, 82, 184102.
503 Schmandt, B., Jacobsen, S.D., Becker, T.W., Liu, Z., and Dueker, K.G. (2014) Dehydration
504 melting at the top of the lower mantle. Science, 344, 1265–1268.
505 Schmerr, N. (2012) The Gutenberg discontinuity: Melt at the lithosphere-asthenosphere
506 boundary. Science, 335, 1480–1483.
507 Song T.R.A., Helmberger, D.V., and Grand, S.P. (2004) Low-velocity zone atop the
508 410-km seismic discontinuity in the northwestern United States. Nature, 427, 530–533.

509 Stolper, E.M., and Ahrens, T.J. (1987) On the nature of pressure-induced coordination
510 changes in silicate melts and glasses. Geophysical Research Letters, 14, 1231–1233.
511 Wakabayashi, D., Funamori, N., and Sato, T. (2015) Enhanced plasticity of silica glass at
512 high pressure. Physical Review B, 91, 014106.
513 Wakabayashi, D., Funamori, N., Sato, T., and Taniguchi, T. (2011) Compression behavior
514 of densified SiO_2 glass. Physical Review B, 84, 144103.
515 Williams, Q., and Garnero, E.J. (1996) Seismic evidence for partial melt at the base of
516 Earth's mantle. Science, 273, 1528–1530.
517 Williams, Q., and Jeanloz, R. (1988) Spectroscopic evidence for pressure-induced
518 coordination changes in silicate glasses and melts. Science, 239, 902–905.
519 Xue, X., Stebbins, J.F., Kanzaki, M., and Trønnes, R.G. (1989) Silicon coordination and
520 speciation changes in a silicate liquid at high pressures. 245, 962–964.
521

522 **Figure Captions**

523 **Figure 1.** Mössbauer spectra of the basaltic glass at high pressures. The spectra were
524 acquired at ambient conditions and 10 ± 2 GPa, 56 ± 7 GPa, 88 ± 2 GPa and 126 ± 2 GPa.
525 The top and bottom ambient spectra correspond to the starting material ("starting") and the
526 recovered sample ("recovered"). All of these spectra were fitted well based on HS Fe^{2+}
527 (gray shaded area) and HS Fe^{3+} (red line) doublets.

528

529 **Figure 2.** QS-CS relations in basaltic glass. The QS and CS values of the present study are
530 compared to those from Dyar et al. (1985). The solid black squares and solid red diamonds
531 show values from the present study on compression for HS Fe^{2+} and HS Fe^{3+}, respectively.
532 The open symbols show the present results of the recovered sample after quenching to
533 ambient conditions. The blue triangles and green squares show the CS-QS values of HS
534 Fe^{2+} and IS Fe^{2+} from Murakami et al. (2012). The gray and red shaded areas ("D85")
535 indicate values for Fe^{2+} and Fe^{3+}, respectively, in various silicate glasses at ambient
536 conditions reported by Dyar (1985).

537

538 **Figure 3.** Pressure dependence of hyperfine parameters of the basaltic glass: (**a**) center shift
539 (CS), (**b**) quadrupole splitting (QS) and (**c**) area ratio of sites in the basaltic glass. The solid
540 black squares and solid red diamonds show values on compression for HS Fe^{2+} and HS Fe^{3+},
541 respectively. The open symbols show the results for the recovered sample.
542
543 **Figure 4.** Mössbauer spectra of the basaltic glass at 1 atm: (**a**) starting basaltic glass
544 acquired at BL11XU of SPring-8, (**b**) sample recovered after quenching from 130 GPa to 1
545 atm.
546
547 **Figure 5.** TEM observations of the basaltic glass recovered from 130 GPa: (**a**) bright field
548 image and (**b**) electron diffraction image of the basaltic glass observed by the TEM. The
549 texture is homogenous and shows no evidence for existence of metallic iron grains. In
550 addition, only a halo pattern from the glass was observed in the diffraction pattern; there are
551 no spots or lines derived from crystalline phases.
552
553 **Figure 6.** Relation between Fe partition coefficient and quadrupole splitting of Fe^{2+}: The

554 upper and lower figures show the pressure dependence of the iron partition coefficient
555 D_{Fe}(solid/liquid) in Andrault et al. (2012) and the QS of HS Fe^{2+} in this study, respectively.
556 The blue and green arrows indicate trends of D_{Fe} and QS, respectively. The dashed lines
557 represent linear least squares fits of each dataset. The solid and open circles show the data
558 on compression and after quenching to ambient conditions, respectively, for Fe^{2+} QS in the
559 present study.

560

561

562 **Table 1.** Composition of basaltic glass.

	[wt%]	563
SiO_2	55.11	± 3.90
TiO_2	0.36	± 0.14
Al_2O_3	14.66	± 0.99
FeO*	9.93	± 1.52
MgO	8.77	± 0.81
CaO	11.33	± 0.84
Na_2O	0.34	± 0.10
K_2O	0.34	± 0.12
Total	100.85	(n = 66)

This is a preprint, the final version is subject to change, of the American Mineralogist (MSA)
Cite as Authors (Year) Title. American Mineralogist, in press.
(DOI will not work until issue is live.) DOI: http://dx.doi.org/10.2138/am-2017-6035

564 **Table 2.** Fitting results of the Mössbauer spectra of the basaltic glass.

Pressure	Fe^{2+}		Fe^{3+}		$Fe^{2+}/\sum Fe$ 565
[GPa]	CS [mm/s]	QS [mm/s]	CS [mm/s]	QS [mm/s]	[%]
0	1.05 ± 0.06	1.88 ± 0.09	0.31 ± 0.03	1.28 ± 0.06	34 ± 14
8 ± 2	1.06 ± 0.05	2.12 ± 0.10	0.35 ± 0.03	1.42 ± 0.06	47 ± 9
10 ± 2	1.05 ± 0.05	2.20 ± 0.12	0.34 ± 0.03	1.42 ± 0.06	31 ± 10
24 ± 2	0.97 ± 0.26	2.54 ± 0.12	0.37 ± 0.12	1.43 ± 0.28	36 ± 18
56 ± 7	0.93 ± 0.13	2.50 ± 0.51	0.33 ± 0.05	1.63 ± 0.15	33 ± 17
75 ± 2	1.04 ± 0.10	2.79 ± 0.21	0.41 ± 0.08	1.74 ± 0.10	20 ± 23
86 ± 2	1.07 ± 0.10	2.64 ± 0.25	0.28 ± 0.06	1.75 ± 0.09	37 ± 20
98 ± 2	1.11 ± 0.21	2.29 ± 0.24	0.23 ± 0.05	1.77 ± 0.11	43 ± 12
103 ± 2	1.09 ± 0.12	2.26 ± 0.11	0.25 ± 0.04	1.75 ± 0.06	28 ± 11
109 ± 2	1.10 ± 0.12	2.37 ± 0.14	0.24 ± 0.04	1.75 ± 0.07	25 ± 19
121 ± 2	1.05 ± 0.07	2.52 ± 0.21	0.25 ± 0.04	1.82 ± 0.06	16 ± 12
126 ± 2	1.03 ± 0.07	2.67 ± 0.17	0.23 ± 0.04	1.79 ± 0.05	20 ± 10
130 ± 2	0.94 ± 0.39	2.86 ± 0.19	0.38 ± 0.14	1.59 ± 0.28	26 ± 20
0 (quenched)	0.99 ± 0.16	2.43 ± 0.72	0.38 ± 0.09	1.20 ± 0.17	21 ± 18

Figure 1

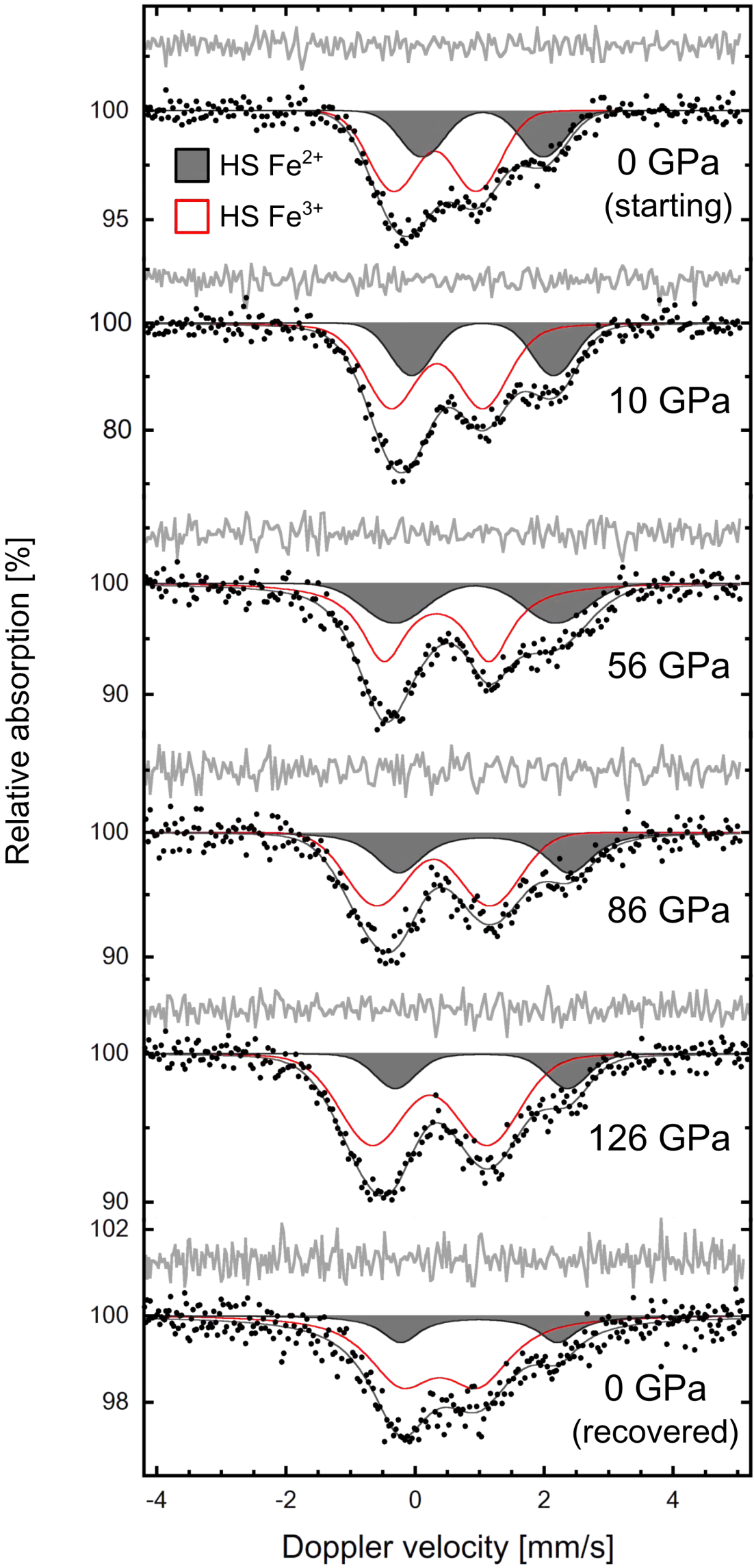
HS Fe2+
HS Fe3+
0 GPa
(starting)
10 GPa
56 GPa
86 GPa
126 GPa
0 GPa
(recovered)
Relative absorption [%]
Doppler velocity [mm/s]

Figure 2

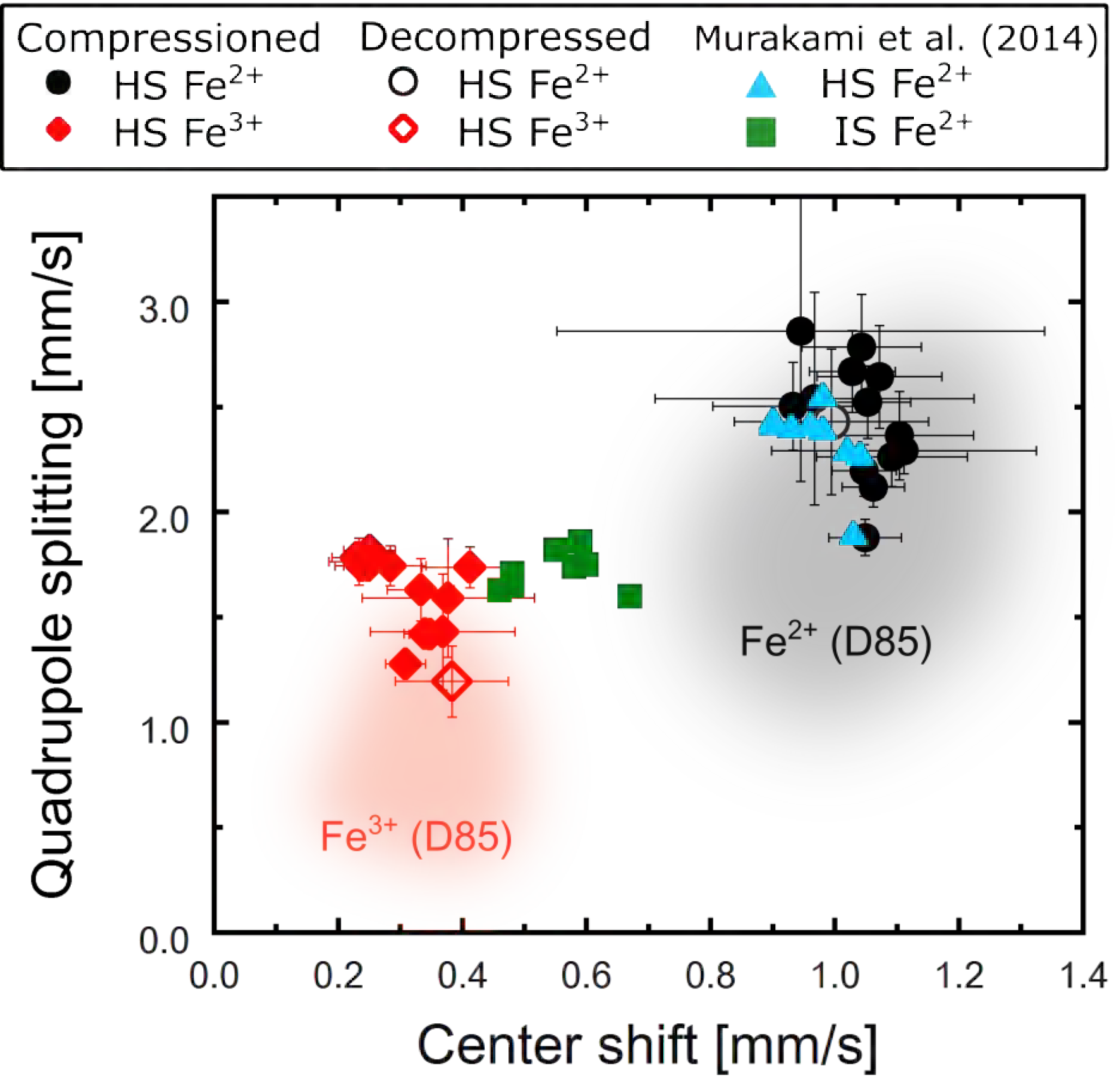
Compressioned
HS Fe2+
HS Fe3+
Decompressed
HS Fe2+
HS Fe3+
Murakami et al. (2014)
HS Fe2+
IS Fe2+
Fe2+ (D85)
Fe3+ (D85)
Quadrupole splitting [mm/s]
Center shift [mm/s]
0.0
1.0
2.0
3.0
0.0
0.2
0.4
0.6
0.8
1.0
1.2
1.4

Figure 3a

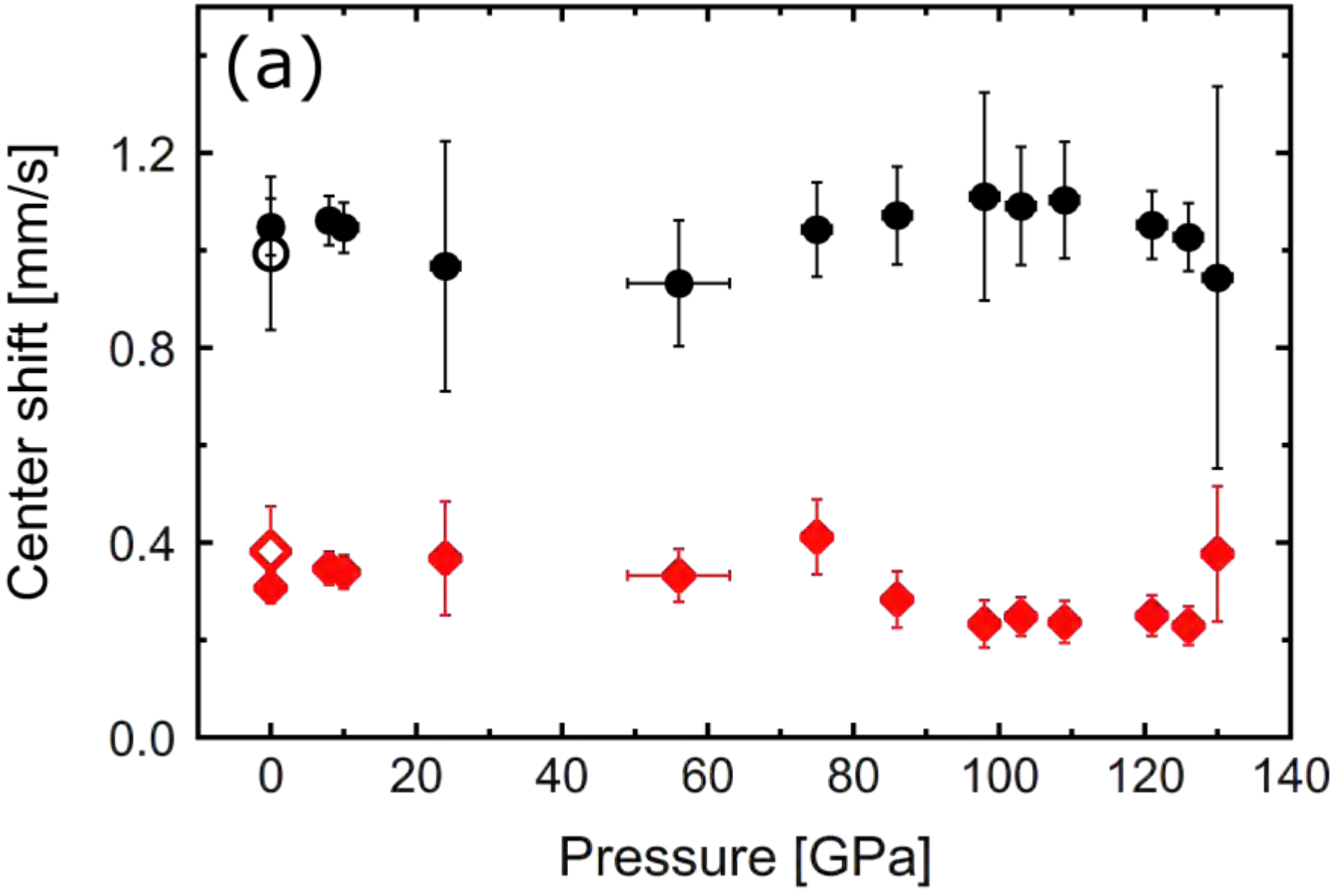
(a)
Center shift [mm/s]
0.0
0.4
0.8
1.2
0
20
40
60
80
100
120
140
Pressure [GPa]

Figure 3b

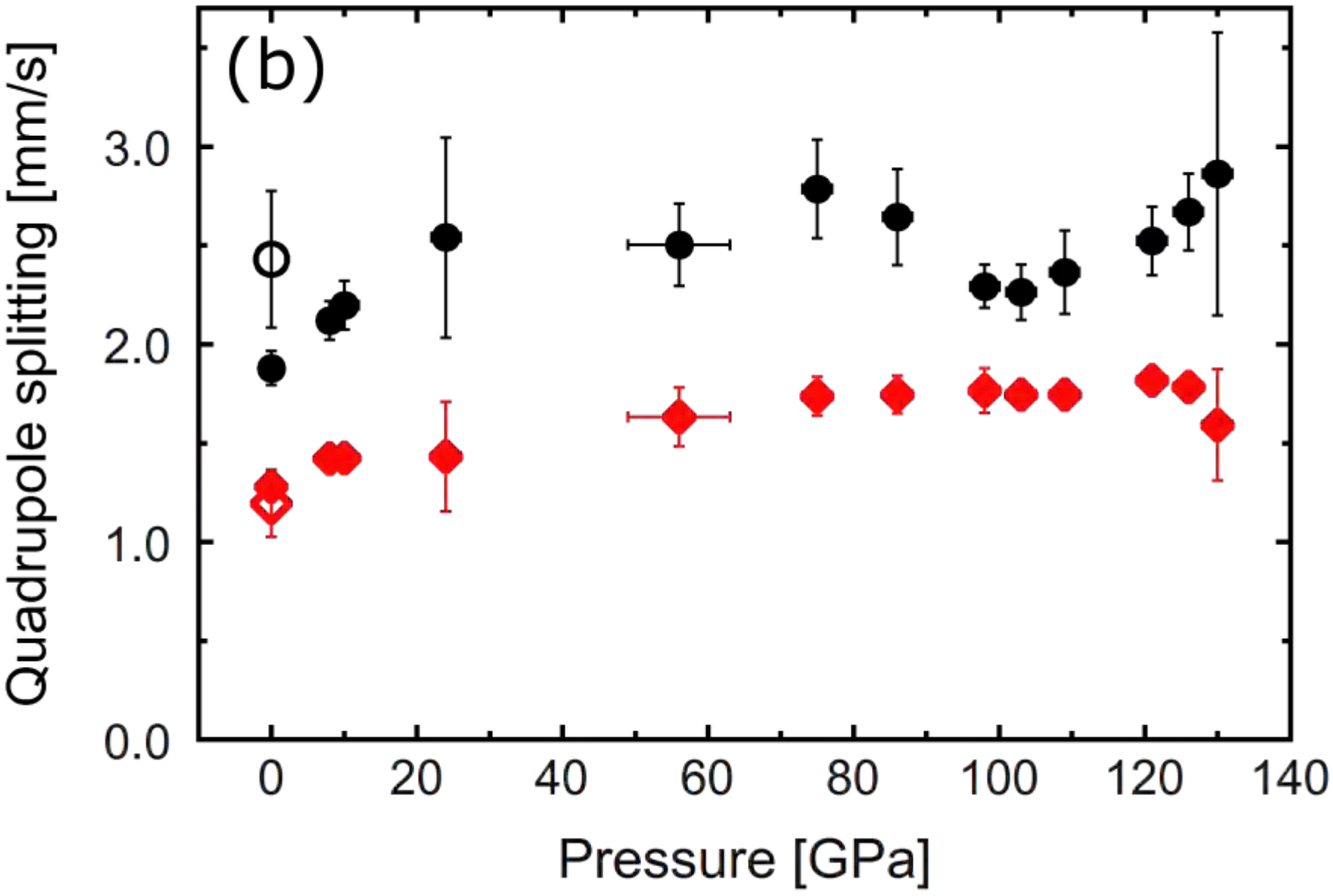
(b)
Quadrupole splitting [mm/s]
3.0
2.0
1.0
0.0
0
20
40
60
80
100
120
140
Pressure [GPa]

Figure 3c

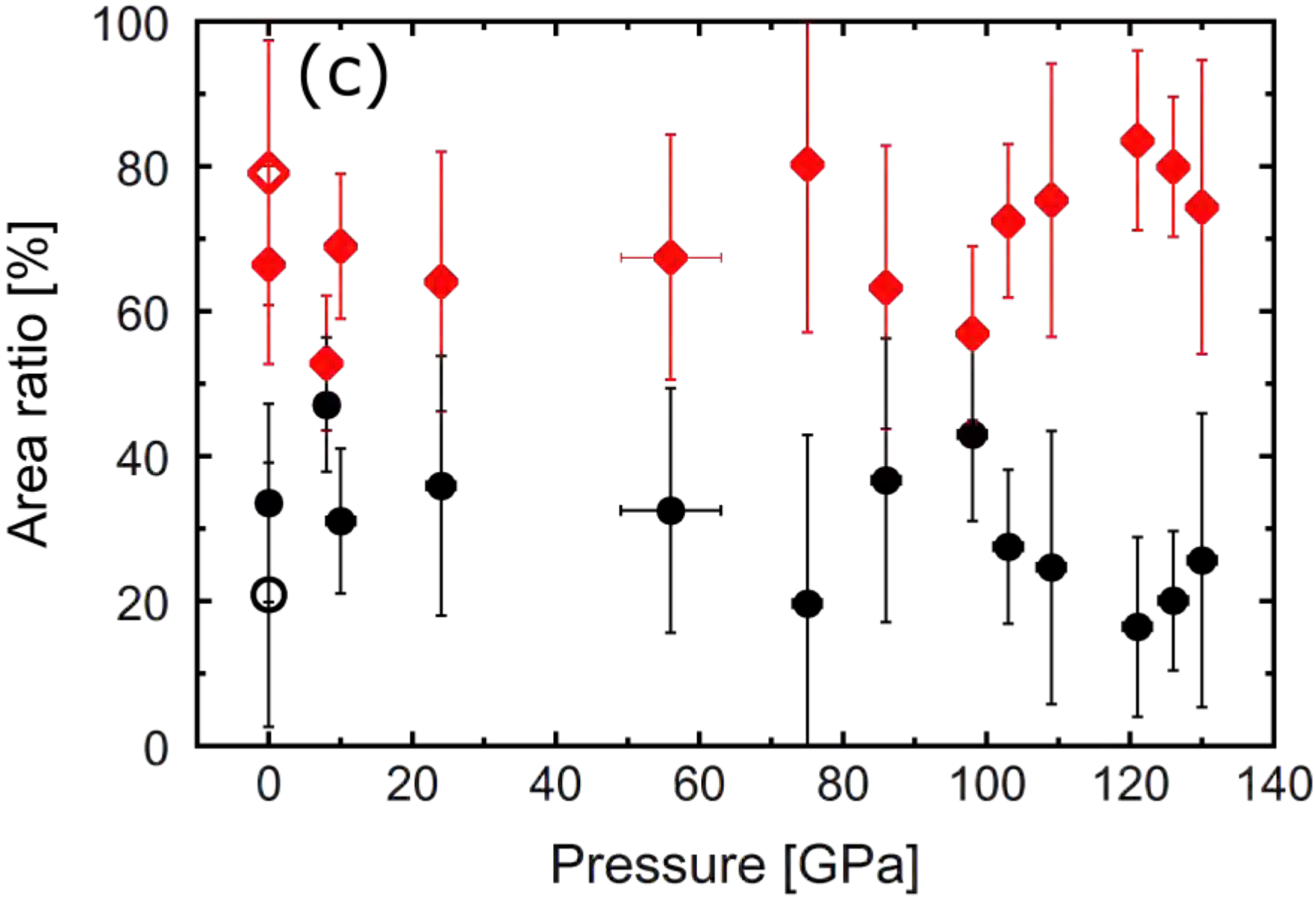

Figure 4

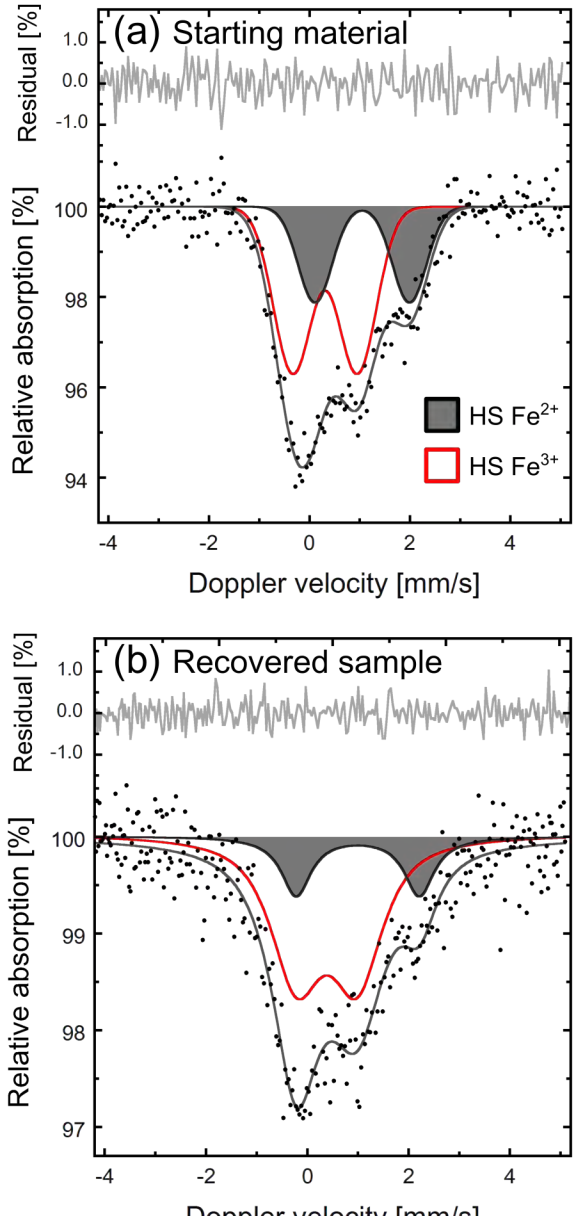
(a) Starting material
Residual [%]
1.0
0.0
-1.0
Relative absorption [%]
100
98
96
94
HS Fe2+
HS Fe3+
-4
-2
0
2
4
Doppler velocity [mm/s]
(b) Recovered sample
Residual [%]
1.0
0.0
-1.0
Relative absorption [%]
100
99
98
97
-4
-2
0
2
4
Doppler velocity [mm/s]

Figure 5

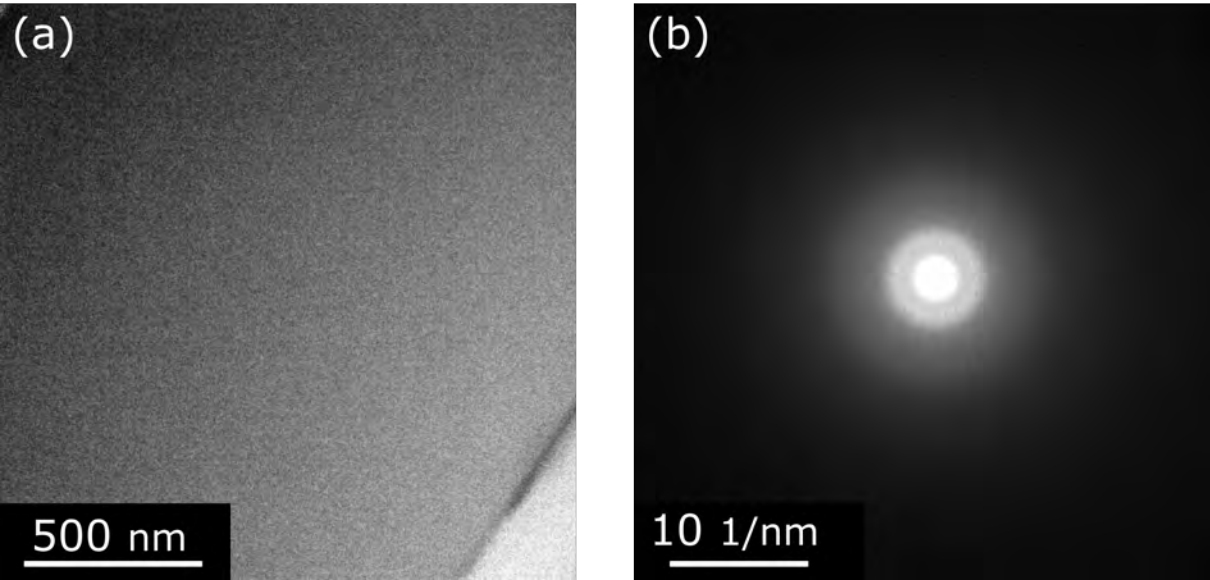

Figure 6

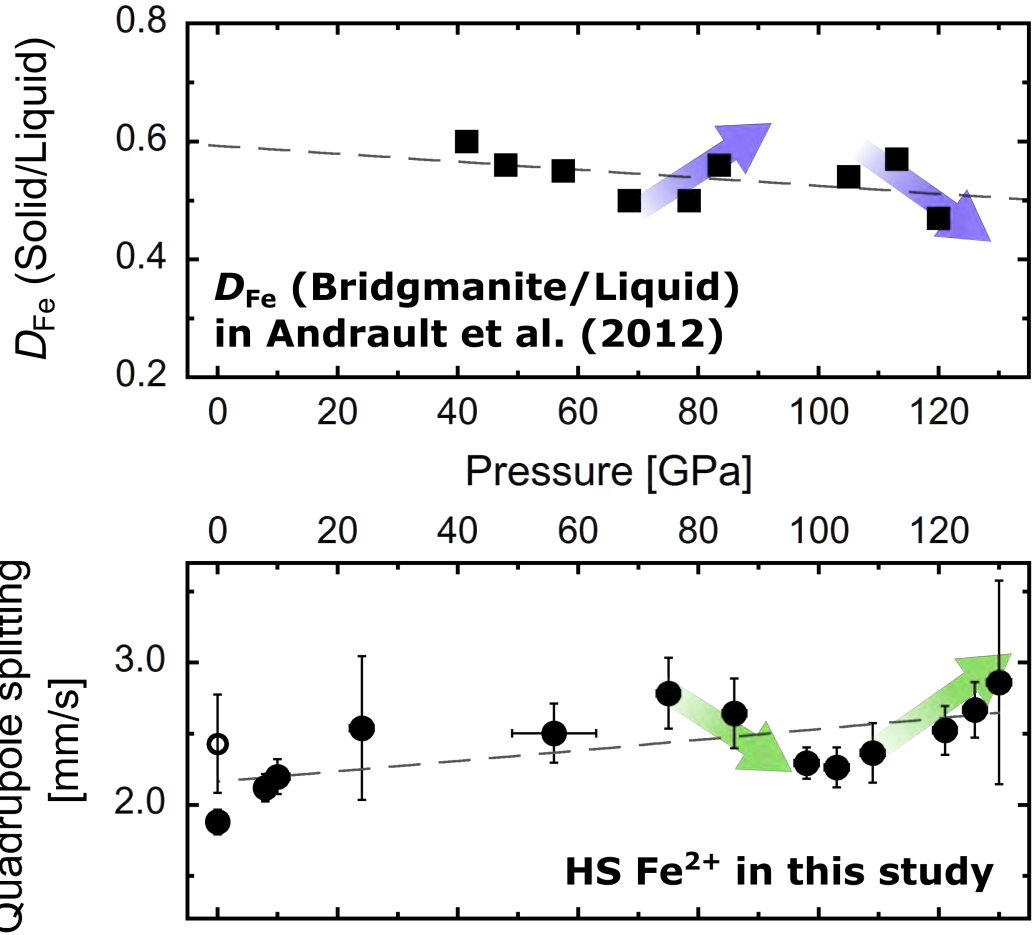
0.8
0.6
0.4
0.2
D_{Fe} (Solid/Liquid)
D_{Fe} (Bridgmanite/Liquid)
in Andrault et al. (2012)
0
20
40
60
80
100
120
Pressure [GPa]
0
20
40
60
80
100
120
3.0
2.0
Quadrupole splitting
[mm/s]
HS Fe^{2+} in this study